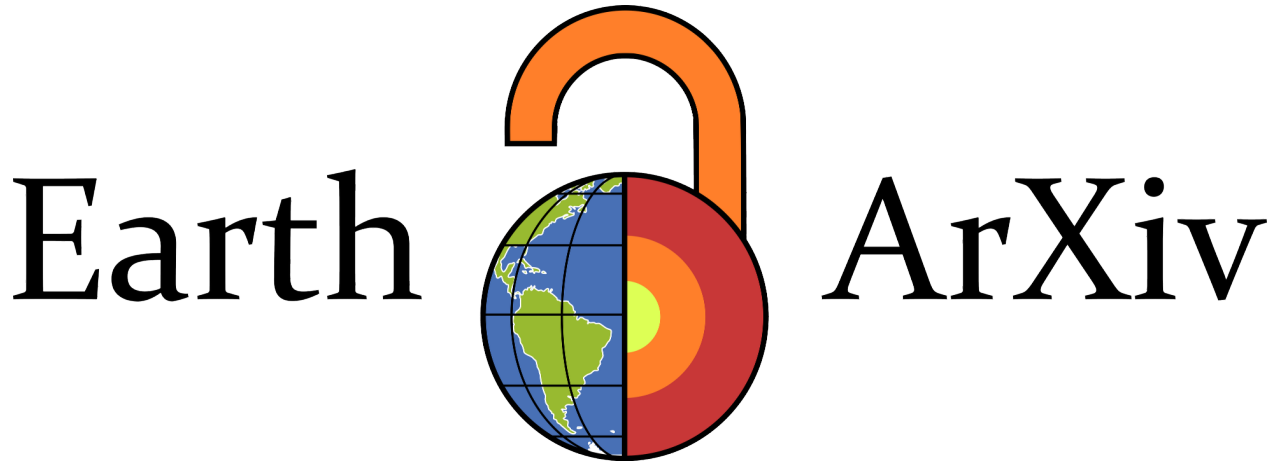

This is a non-peer-reviewed preprint submitted to EarthArXiv.

Please note the manuscript has yet to be formally accepted for publication. Subsequent versions of this manuscript may have slightly different content. If accepted, the final version of this manuscript will be available via the 'Peer-reviewed Publication DOI' link on the right-hand side of this webpage. Please feel free to contact any of the authors; we welcome feedback.

Multi-proxy approach in tracking circulation change in the western North Atlantic during the Little Ice Age

Wai Ching Rachel Chu[1,2], Benoit Thibodeau[1]

[1]Department of Earth and Environmental Sciences & School of Life Sciences, The Chinese University of Hong Kong, Sha Tin, N.T., Hong Kong S.A.R.

[2]Now at School of Ocean and Earth Science, Faculty of Environmental and Life Science, University of Southampton, Southampton, SO17 1BJ, United Kingdom

Corresponding authors:

Wai Ching Rachel Chu; Email address: wcrachel@link.cuhk.edu.hk

Benoit Thibodeau; Email address: benoit.thibodeau@link.cuhk.edu.hk

ABSTRACT

The Little Ice Age (LIA), a period from ~1400 CE to 1900 CE, was characterized by colder winter and more frequent extreme weather event, particularly in the Northern hemisphere. While the exact causes of the Little Ice Age remain a topic of ongoing research, evidence suggests that changes in ocean circulation patterns likely played a role in the observed global cooling, although the specific mechanisms and drivers of these changes are not yet fully understood. Here, we aim to generate new knowledge to help us better understand how ocean circulation changed before, during, and after this climatic event. To do this, we will investigate changes in the western North Atlantic circulation that can inform us on the relative strength of the Labrador current and Gulf stream. First, we established Mg/Ca-temperature calibration curve for *Globobulimina auriculata* in the Lower St. Lawrence Estuary, i.e. $Mg/Ca\ (mmol/mol) = 0.6341e^{(0.3740t)}$ for bottom water temperature reconstruction. Coupling the temperature reconstruction with oxygen isotope data, we reconstructed the relative strength of the Labrador current and Gulf stream to infer regional oceanographical change. We discussed the oceanographic changes during the LIA in respect to volcanism, solar irradiance, and North Atlantic Oscillation. Additionally, we noted similarities between our records and previous proxy interpretations on the strength of Atlantic Meridional Overturning Circulation (AMOC), the Gulf Stream, and the Labrador Current. Our interpretation suggested a stepwise weakening of AMOC throughout the LIA followed by a sharp decrease of the oxygen isotope likely driven by a freshwater release.

Keywords

Mg/Ca ratio, foraminifera, oxygen isotope, St Lawrence Estuary, temperature reconstruction, Little Ice Age, Labrador Current, Gulf Stream, AMOC, Paleoceanography

INTRODUCTION

The Little Ice Age (LIA) is a relatively short climate anomaly (~1400-1900 CE, with variable onset timing depending on the region), characterized by abrupt cooling and glacier expansion, following the warming in Medieval Climate Anomaly (MCA) (Brönnimann et al., 2019; Wanner et al., 2022). LIA was the coldest period in the last 8,000 years, being 0.7 – 1°C cooler in the Northern Hemisphere compared to 2000 CE (Lean and Rind, 1999). It is also associated with a higher frequency of extreme weather and more extreme seasonal temperatures. Due to the higher land coverage, the northern hemisphere was suggested to be more affected than the southern hemisphere (Wanner et al., 2022). Interestingly, the socio-economic impacts of the LIA have been relatively well-documented (e.g., Behringer 1999; Fan 2023; Putnam et al. 2016), which makes it a valuable area of interest for understanding how abrupt climate may affect our livelihoods. While it is not a climate analog *sensus stricto*, it may provide valuable insight into ocean-climate interactions and feedback during a relatively abrupt climate shift. Its late occurrence provided us with relatively high resolution in the sedimentary records. While the dominating factors causing the onset of LIA are poorly understood, previous study suggest that atmosphere-ocean feedback may have played an important role (Moffa-Sánchez et al. 2019).

In the North Atlantic Ocean, the saline surface water of the North Atlantic current flows northward and gradually loses buoyancy by cooling, to a point where it is denser than the subsurface water and sinks, forming a deep overturning cell in the sub-polar Atlantic that drives thermohaline circulation (Buckley and Marshall, 2016; Ferreira et al., 2010). This part of the overturning circulation is often referred to as the Atlantic Meridional Overturning Circulation (AMOC). The Gulf Stream and the Labrador Current are two of the ocean currents constituting the AMOC and are part of the North Atlantic subpolar gyre (Figure 1).

The Gulf Stream is a northeastward-flowing warm surface current originating in the Gulf of Mexico, bringing heat up the meridians while the Labrador Current is a cold surface current flowing southward along the North Atlantic coast under the Coriolis force. Their respective strengths have been used as proxies to discuss changes in the strength of AMOC in various periods, such as the Holocene and the modern times (Ezer, 2015; Rashid et al., 2017; Thibodeau et al., 2018, 2010). While the strength of AMOC experienced variations of large amplitude during Earth's history, less dramatic variations are often overlooked and may be as informative about the potential consequences of global warming on AMOC(Galaasen et al., 2020).

During the LIA, changes in the AMOC may have impacted meridional heat transfer to higher latitude, which might have affected North Atlantic and sub-polar regions climate (Moffa-Sánchez et al. 2014). Multiples study attempted to resolve changes in AMOC and identify its drivers during this period (Table 1.); two different mechanisms were proposed to explain changes in AMOC, i.e. wind forcing and freshwater forcing. In the wind forcing scenario, the negative North Atlantic Oscillation caused a weaker Northwestern wind and more frequent Southern wind, leading to a weaker Labrador Current, which is also associated with a northward shift in the Gulf Stream (Jutras et al., 2023; Sicre et al., 2014), thus resulting in a weaker AMOC. On the other hand, in the freshwater forcing scenario, the increase in storminess (Dawson et al., 2007) during LIA caused more sea ice to be breaking off and rafting, before eventually melting and contributing to the Labrador Current. The large quantity of freshwater decreased the salinity, lowering the density gradient and thus weakening Labrador Sea convection and the subpolar gyre convection, resulting in a decreased AMOC (Alonso-Garcia et al., 2017; Holliday et al., 2020; Moffa-Sánchez et al., 2014; Moffa-Sánchez and Hall, 2017; Rashid et al., 2023; Thibodeau et al., 2018, 2010;

105 Thornalley et al., 2018). With a consensus on having both forcings contributing to a
106 potentially weaker AMOC, debates were drawn on which forcing was more predominant
107 (Moffa-Sánchez et al. 2014; Sicre et al. 2014), which could potentially be unraveled by
108 determining the strength of the Labrador Current during the LIA. The freshwater hypothesis
109 would support a stronger Labrador Current (Sicre et al. 2014; Rashid et al. 2023). On the
110 other hand, the wind stress hypothesis would imply that more freshwater was entering
111 through the Fram Strait, thus strengthening the East Greenland Current and weakening the
112 Labrador Current as a result (Jutras et al., 2023).
113 Previous reconstructions of NW Atlantic oceanography during the LIA proposed an increase
114 in the relative contribution from the Gulf Stream on the Eastern coast of Canada based on
115 oxygen isotope records from benthic foraminifera (Thibodeau et al. 2018). However,
116 the temperature and salinity signal from the results cannot be disentangled solely from the
117 oxygen isotope proxy. Here, we have produced new Mg/Ca data from benthic foraminifera to
118 serve as a temperature proxy to disentangle the contribution from change in water masses in
119 the oxygen isotope signal. We aim to provide new insights into the oceanographical changes
120 happening in the NW Atlantic during the LIA and thus contribute to a better understanding of
121 the relationship between AMOC, the subpolar gyre, and climate.

122

123 Magnesium-to-Calcium (Mg/Ca) ratio in carbonates is a commonly used paleothermometer
124 with increasing popularity (e.g. Stirpe et al. 2021; Barrientos et al. 2018; Evans et al. 2018;
125 Rustic et al. 2021; John et al. 2023). While the Mg/Ca ratio in perforate foraminiferal tests is
126 determined both biologically and by the chemical properties of ambient seawater (Bentov and
127 Erez, 2006; Erez, 2003), its high dependence on temperature makes it a suitable
128 paleothermometer. The temperature correlation can be deduced from biological (Bentov and
129 Erez, 2006) and physical factors (Alkhatib et al., 2022; Katz, 1973; Mucci, 1987; Rosenthal

et al., 1997). The solubility of calcite decreases with increasing temperature (Segnit et al., 1962), and more Mg^{2+} is incorporated into inorganically precipitated calcites with increasing temperature. For the biological factors, temperature enhances ATP hydrolysis, i.e. a chemical process transforming ATP to ADP and energy. Since ATP molecules can bind free Mg^{2+} ions, an enhanced ATP hydrolysis would mean having less ATP available and subsequently having less Mg^{2+} ion to be bound by ATP, causing the concentration of free Mg^{2+} ion in the cellular environment to increase thus increasing the Mg/Ca ratio. Another biological factor of the Mg/Ca ratio relies on the diffusion constant for the Mg^{2+} ion, which increases with temperature, meaning a quicker diffusion between ambient seawater and the privileged space in the vacuole of the foraminifer (Bentov and Erez, 2006).

Therefore, this paper uses measurements from single foraminifer ICP-MS to establish a Mg/Ca- temperature calibration curve for *Globobulimina auriculata* in the lower St. Lawrence Estuary. By removing the temperature signal from oxygen isotopic data, we reconstructed the relative proportion or Labrador Current and Atlantic water entering the Laurentian channel in order to better understand the dynamic of these water masses during the LIA.

METHODOLOGY

Sediment core and subsampling

Two sediment cores collected from the St. Lawrence Estuary were used in the experiment (Figure S1). Core CR02-23 is a 0.12 m^2 x 0.5 m long core collected at 48º42.008'N, 68º38.894'W, via the expedition on R/V Coriolis II in 2002 CE. The age-depth model of the core was previously established using Pb-210 (Thibodeau et al., 2010, 2006). A 1.8-yr age uncertainty was calculated in the age model (Figure S2). Five cc of wet sediment was taken at

a 1-cm interval, from 0 cm – 30 cm, with an additional sampling at 0.5 cm depth. The depth corresponded to 1933 – 2001 CE. The average sediment rate was 0.42 cm/yr. Analyses on this CR02-23 core were used for establishing a Mg/Ca – temperature calibration equation.

The second core MD99-2220 is a 51.6m long core, collected at 48°38.32N, 68°37.93W, 320 m depth. It was obtained via the use of Calypso piston corer during the excursion in 1999 CE at the R/V Marion Dufresne. The first 14cm of the core was missing due to the disturbance of the corer to the sediment surface (St-Onge et al., 2003). This core had been divided into two units: Unit 1 (base till 1497 cm); Unit 2 (1497 cm till the surface). Unit 2 was characterized by the overall presence of postglacial bioturbated silty clay. The age-depth model was previously established using radiocarbon (St-Onge et al., 2003). Five cm^3 of wet sediment was taken from the core at an 1-cm interval, from 0 cm – 75.5 cm of Unit 2, with an addition sampling at 0.5 cm depth. The depth corresponded to 1396 – 1975 CE, i.e. the section covering the LIA (Figure S3). The literature sedimentation rate was 0.74 cm/yr for 0-20 cm, 0.28cm/yr for 20-30 cm; 0.15cm/yr for 30 – 75 cm (St-Onge et al., 2003). The age uncertainty was set as 2σ of the ^{14}C dating, i.e. ± 100 yr. Analyses on this MD99-2220 core were used for oceanographic interpretations during the LIA.

Wet sediment was sieved through a 63-μm sieve to remove clay, while retaining the foraminifera species. *Globobulimina auriculata* was identified under the Leica EZ4W Stereomicroscope and hand-picked using a moist brush. Depending on the availability of individuals available, four intact foraminifera were selected from each depth as replicates (Trejos et al., 2003).

Cleaning and Dissolution

The tests were cleaned individually following the protocol from Barker, Greaves, and Elderfield 2003, without the reductive cleaning step in the procedure. The original aim of

reductive cleaning was to remove the Mn-oxide coatings (Martin and Lea, 2002). While previous study observed a 10-15% Mg/Ca ratio decrease after reductive cleaning, only a 0.03 mmol/mol (i.e. 1%) decrease of Mg/Ca was expected if all Mn-Fe oxide coating was removed (Barker et al., 2003). Given that Mg/Ca ratio obtained from this foraminifer specie is low, i.e. average 3.65 mmol/mol, we did not include a reductive cleaning step to avoid excessive Mg/Ca ratio loss.

Single-foraminifer ICP-MS Analysis

We used JCp-1, a certified coral reference material developed by the Geological Survey of Japan, as internal standard. It was chosen because of its marine calcite nature and reference of use in other foraminiferal studies (e.g. Zhou et al. 2022; Yoshimura et al. 2011). Self-made multi-element solution (MeRC) was used as a reference material with the mix of pure Ca, Mg, Sr, Mn and Fe solutions and blank. The accuracy and precision (<5%) of MeRC was measured via the use of ICP-MS prior to use. Each run of the ICP-MS analysis was composed of 2% nitric acid blank acquisition at the start and end of the run. Every five foraminiferal sample acquisitions were accompanied by a set of reference material and 2% nitric acid blank for recalibration and brief cleaning of the machine. Details of the ICP-MS set-up can be found in the supplementary information.

Raw data were obtained from the ICP-MS Data Analysis window software (Agilent Technologies, 2014). Since ICP-MS can be relatively unstable, frequent recalibration of the machine against reference materials is needed (Jackson and Sylvester 2008). Re-calibration was done with MeRC correction, in which the cps of each elemental isotopes in the first MeRC acquisition of each run was used as the baseline. These baseline cps values were then compared against the subsequent MeRC acquisitions within the same run. The variations between each MeRC acquisition and the baseline were calculated and then a linear slope was

calculated between the MeRC acquisitions. The samples in between the acquisitions were corrected with the respective slope. To counteract the effects of not applying a reductive cleaning step, data exceeding the elimination threshold were considered contaminated. The elimination threshold was listed in Table S2.

CR02-23 Calibration Curve and Temperature Reconstruction Comparison

Using the MeRC-corrected $^{24}Mg/^{48}Ca$ data and instrumental temperature obtained from Thibodeau et al., 2018, calibration curves were established and compared with both linear fit and exponential fit. With the $^{24}Mg/^{48}Ca$ data, bottom water temperature was also reconstructed and compared using the calibration equations from:

1) Anand, Elderfield, and Conte 2003, a universal Mg thermometry equation has been attempted by using paired Mg/Ca and $\delta^{18}O$ measurements in 11 planktic foraminifera species:

$$Mg/Ca\ (mmol/mol) = (0.38 \pm 0.02)\ e^{((0.090 \pm 0.003)t)}$$

t represents water temperature in Celsius

2) Lear, Rosenthal, and Slowey 2002, a general calibration equation for benthic foraminifera from a core-top calibration of common *Cibicidoides* species:

$$Mg/Ca\ (mmol/mol) = (0.867 \pm 0.049)\ e^{((0.109 \pm 0.007)t)}$$

t represents water temperature Celsius

3) Weldeab, Arce, and Kasten 2016, a linear calibration curve for the genus *Globobulimina*:

$$Mg/Ca\ (mmol/mol) = (0.36\ \pm 0.02)t + 2.22 \pm 0.19$$

t represents water temperature in Celsius

230

231 *Salinity Effect*

232 The matter of whether salinity affects Mg/Ca ratio in foraminifera is under debate, especially
233 for benthic foraminifera (e.g. Mathien-Blard and Bassinot 2009; Weldeab, Arce, and Kasten
234 2016). To investigate the possibility of observing a salinity effect on our Mg/Ca data, two
235 methods were tested. 1) Mg/Ca data was analyzed against the instrumental 300m bottom
236 water salinity data from the Canadian Government (Galbraith et al., 2018); 2). Differences
237 between our Mg/Ca data and back-calculated Mg/Ca data from Weldeab, Arce, and Kasten
238 2016 equation, in which they solely observed a temperature effect from the calibration of
239 *Globobulimina sp*., was analyzed against instrumental salinity:

240

241 $$Mg/Ca\ (mmol/mol) = (0.36\ \pm 0.02)t + 2.22 \pm 0.19$$

242 *t represents water temperature in Celsius*

243

244 **MD99-2220 Parent Water Mass Reconstruction**

245 After establishing a calibration curve from CR02-23, Mg/Ca data from MD99-2220 was
246 input into the established curve for bottom water temperature reconstruction. Alongside the
247 literature $\delta^{18}O_{(calcite)}$ data previously obtained for MD99-2220 (Thibodeau et al. 2018), we
248 could calculate the $\delta^{18}O_{(seawater)}$ signal from the equation below from the Marchitto et al.,
249 2014, assuming an 0.9 ‰ offset for vital effect, which was the offset value observed in
250 *Globobulimina affinis* (Hoogakker et al., 2010):

251 $$t\ (^{o}\ C) = \frac{0.245 - \sqrt{0.045461 + 0.0044(\ \delta^{18}O\ _{(calcite)} - \delta^{18}O\ _{(seawater)})}}{0.0022}$$

252 *t represents water temperature in Celsius*

Given that ATSW and LSSW have their distinct $\delta^{18}O$ signal, we can track the change of contribution via $\delta^{18}O_{(seawater)}$ changes (Thibodeau et al. 2018; Thibodeau et al. 2010). In the $\delta^{18}O_{(seawater)}$ signal reconstruction, a more positive signal represents a more dominant ATSW (proxy for Gulf Stream) and a more negative signal represents a more dominant LSSW (proxy for Labrador Current). A 95% confidence interval was applied for all statistical analyses, and all results were corrected to two decimal places, apart from cps, R-squares, and equations. All analyses and graphs were produced on GraphPad Prism 9.0 and Excel, while maps were produced via the use of Ocean Data View.

RESULT

CR02-23

Regarding the analyses done on Core CR02-23, 75 foraminiferal measurements were made across three runs (i.e. on 2023-10-06, 2023-10-13 and 2023-10-20). All elemental isotopes measured had values higher than LOD and LOQ thus representing a quantifiable concentration in the samples.

Mg/Ca Ratio

After applying the elimination threshold described in the methodology section, 43 measurements remained for data analysis. Obtained foraminiferal $^{24}Mg/^{48}Ca$ ranges from 1.72 to 9.01 mmol/mol (Table S3). The p-value for the linear regression model for the isotope ratios was lower than 0.05, representing a significant relationship between bottom water temperature and Mg/Ca ratio (Figure 2a). For both linear and non-linear (exponential) models, the R-squared values obtained were both higher than 0.7, both representing a strong

correlation between temperature and Mg/Ca ratio (Table S4). The exponential equation is favoured from this result since it displayed a slightly higher R-square value than the one obtained from linear equations.

Salinity Effect and contamination

For salinity, the p-value was larger than 0.05 thus the equation was not statistically significant (Figure 2b). R-squares are lower 0.2, representing a weak correlation between salinity and Mg/Ca (Table S5). However, the lack of correlation could be the result from the smaller sample size (n=8) and narrow salinity range (32.34 to 34.94 psu) because of the limited salinity record during the study period. No significant correlation was observed between Mn/Ca or Fe/Ca with Mg/Ca (Figure 3). A low but significant correlation was found between Al/Ca and Mg/Ca. Since the correlation was low, we considered that little contamination affected the samples.

MD99-2220

A total of 286 foraminiferal samples were analysed. After applying the elimination threshold and eliminate analysis with accuracy and precision over 20%, 100 measurements remained for data analysis.

The average Mg/Ca ratio in MD99-2220 across depths 0 cm to 76 cm ranged from 1.14 to 9.16 mmol/mol. After bottom water reconstruction, a temperature range of 1.58 to 7.18°C was reconstructed (Figure 4a). We observed a stepwise increase in temperature from ~1396 to 1905 CE, followed by a decrease from ~1905 CE onwards.

The seawater isotope signal dropped from the start of the record until ~1500 CE, then the signal followed a stepwise increase until ~1870 CE, followed by a sharp decrease (Figure

4b). Because of the relatively high standard deviation of our measurements, caution was used when discussing smaller variations in our record.

DISCUSSION

Calibration of Mg/Ca vs temperature in the St. Lawerence Estuary

Comparisons of Previously Established Calibrations

Using our CR02-23 Mg/Ca ratio data in previously established calibration equations, as visually presented in Figure 5, served the purpose of not only testing the applicability of these equations to our reported species and location, but also testing whether the range of the Mg/Ca ratio obtained would be within a normal temperature range thus proving the validity of the result and thus the methodology. We can observe that calibration curves created using planktic foraminifera, other species of benthic foraminfera or same genera of foraminifera but from a different location do not yield realistic temperature compared to our environment (3.1 to 5.38 °C). Therefore, this explicitly call for a new regional calibration curve using *Globobulimina auriculata.*

Calibration Equation for Globobulimina auriculata at Lower St. Lawrence Estuary

The calibration equation was established as the best-fit exponential equation from $^{24}Mg/^{48}Ca$ data after MeRC correction and instrumental temperature from the St. Lawrence bottom water (Thibodeau et al., 2018), i.e.

$$Mg/Ca\ (mmol/mol) = 0.6341e^{(0.3740t)}$$

t represents water temperature in Celsius

This equation was established for a bottom water temperature range of ~3.0 to 5.5°C, with an R-square of 0.76. The R-squared value of a curve, which varies from 0 to 1, can explain how well the data fit the model. The larger the value, the better the curve fits the data. An R-square value of 0.76 is generally considered as a strong positive relationship between Mg/Ca ratio and temperature. It is important to note that this calibration uses Mg/Ca values based on our chronostratigraphy and instrumental temperature based on real calendar years and thus the R-square of 0.76 include the uncertainty linked to the chronology and thus may be lower than traditional laboratory-based calibration. Moreover, since instrumental temperature data was not frequently collected and the collection did not start until the 1930s (Thibodeau et al. 2018; Galbraith et al. 2018), we can only rely on data within a 2 °C temperature range for the reconstruction. While this model can provide a finer scale reconstruction, the narrow temperature range will amplify the deviation between the actual data and model data, thus resulting in a relatively lower R-square value. Finally, carbonate ion may not affect our record as it was suggested that carbonate ion concentration would affect Mg/Ca ratio only when the bottom water temperature is lower than ~3 °C (Elderfield et al. 2006), which is out of the temperature range of this study.

Therefore, despite some potential limitations in establishing a Mg/Ca-temperature calibration for palaeothermometry, we have proposed a relatively robust calibration equation tailored to *Globobulimina auriculata* at the Lower St. Lawrence Estuary that should be useful to generate new knowledge regarding the dynamic of western North Atlantic circulation during the LIA.

Little Ice Age temperature reconstruction

We observed that changes in bottom water temperature reconstructed from our Mg/Ca data followed the same pattern as the parent water mass contribution change (calculated from the

351 $\delta^{18}O$ stripped from temperature effect, Figure 4b). Because these two water masses are
352 characterized by different temperature, it is reasonable to believe that the dominant factor
353 controlling the observed temperature changes is the change in parent water mass contribution
354 to the lower St. Lawrence Estuary, assuming a constant isotopic signature throughout this
355 period. To divide the core into smaller time intervals for interpretations, non-parametric
356 Mann-Kendall Trend Test was applied via the use of RStudio to observe potential significant
357 trends. A significant positive trend was observed from 1490 to 1850 CE for both
358 reconstructed oxygen isotope and temperature (Table S6). Divisions were drawn in 1490 and
359 1850, such that three time-intervals were identified in the timeline (Figure 6). In the
360 following sections, we will discuss the trends in these time intervals, to single out potential
361 drivers of change in the dynamic of Northwestern Atlantic circulation during LIA.

362

363 *Transition from MCA to LIA (1396 to 1490 CE)*

364 This time interval was characterized by a relatively constant signal, followed by a relatively
365 sharp decrease in both temperature and oxygen isotope in ~1470-1500. A large stratospheric
366 sulphur loadings from explosive volcanic activities was reconstructed from ~1275 to 1300
367 CE (Miller et al., 2012), before the onset of LIA. The sulphate aerosols from the increasing
368 volcanic activities absorbed solar radiation in conjunction with the reduced solar irradiance
369 from the Spörer Minimum from 1440 to 1460 CE (Lean and Rind, 1999). Interestingly, these
370 events happened right before the drastic change in parent water mass/ oxygen isotope
371 observed in our record in ~1470-1500. The combined effect could not only cause a short-
372 lived cooling effect that was more obvious in summer (Miller et al., 2012), but also more
373 extreme weather (Brönnimann et al., 2019). The latter was evidenced by the increasing
374 storminess (suggested by an increase in Na^{+}) observed in GISP2 ice core around ~1400 CE

375 (Dawson et al. 2007; Mayewski et al. 1997; Trouet, Scourse, and Raible 2012), which was
376 later interpreted as an increase in intensity of storms during LIA (Knudsen et al., 2014). The
377 extreme weather conditions may lead to the increase fracturing and break-up of sea ice due to
378 strong winds. The broken sea ice then melted and entered the Labrador Current through the
379 Canadian Archipelago Route as freshwater. In addition, remaining meltwater supply from the
380 warm Medieval Climate Anomaly (MCA) could increase the freshwater supply to the
381 Labrador Current (Moffa-Sánchez et al. 2014; Lapointe and Bradley 2021). This sudden
382 increase in freshwater discharge could potentially explain the initial strengthening of the
383 surface and sub-surface Labrador Current. This freshwater would also bring cooler
384 temperature, which was observed around ~1350 CE from TEX_{86}-T result (Rashid et al.,
385 2023). This cooling was accompanied by an increase in the size of sortable silt from
386 Southeast Grand Banks suggesting an increased Labrador Current flow speed since ~1450
387 CE, right before the increase in the contribution of LSSW observed in our record (~1470-
388 1500 CE). Concurrently, the lower solar irradiance from extreme volcanism and solar minima
389 might have caused a reduced northward heat transport causing a southward shift in ITCZ
390 and then a southward shift in the Gulf Stream (Lund et al., 2006). This shift may contribute to
391 the lower contribution from ATSW in our record. The reduced heat transport would also be
392 coherent with the temperature-based AMOC index (Figure 7) which dropped at the same
393 time, probably partly because of the weakening of the ATSW branch. Taken all evidence
394 together, it suggests that, in this time interval, external forcing like increased volcanism and
395 reduced solar insolation might have led to the observed increased contribution of LSSW in
396 our record, and decreased contribution of ATSW, through high-latitude freshwater input and
397 reduced heat transport respectively.

398

399 *Little Ice Age (~1491 to 1870 CE)*

This time interval recorded the LIA in the study region and was characterized by a statistically significant increasing trend of both the oxygen isotope signal and bottom water temperature, evidenced by the Mann-Kendall test result (Table S6). The coldest and freshest water observed in a previous study in the subsurface Labrador Sea was recorded in around ~1580 CE, based on the Mg/Ca- $\delta^{18}O$ analysis of *Neogloboquadrina pachyderma* (Thornalley et al., 2018) and that a surge of cold and fresh subsurface water was identified around ~1620 CE from the $\delta^{18}O$ *Turborotalita quinqueloba* result (Moffa-Sánchez et al. 2014). Therefore, the lower bottom water temperature and the stronger contribution from LSSW at the start of this time interval, can be interpreted as the indicator of a strong surface and sub-surface Labrador Current and a weak contribution from ATSW, which could be a direct continuation of the cold conditions created by previous external forcing, with a stabilisation of the strong influence of the Labrador current in the Northwestern Atlantic and a reduced Gulf stream.

Later in this period, the contribution of the ATSW increases (Fig 4b). A more saline Gulf Stream was reported in ~1750 CE, from dryer conditions in North Atlantic that was caused by a more negative North Atlantic Oscillation (NAO^-) (Lund et al., 2006; Saenger et al., 2009). A more saline Gulf Stream would also lead to a higher oxygen isotope signal in water from the Gulf Stream (ATSW), contributing to the increasing oxygen isotope signal in our reconstruction. Moreover, NAO^- would cause weaker NW winds and more frequent southerly winds (Sicre et al., 2014). With the change in wind stress, the weaker NW winds push less sea ice debris down the Canadian Archipelago Route (West of Greenland). This, in turn, would lead to a decrease in discharge supply and strength of Labrador Current. This is coherent with an observation of increased flow through the Fram Strait (Perner et al. 2011) where they used their observation of the highest abundance of agglutinated Arctic water species at ~1650 CE, as the indicator of increasing water entering from the Fram Strait

instead of the Canadian Archipelago. While this may contribute to a decrease in the Labrador Current, the lower freshwater input may favour an increase in the formation of deep water in the Labrador Sea basin because of a higher salinity gradient (Holliday et al., 2020), which is coherent with a delayed increase in the reconstruction of the deep western boundary current (DWBC) in ~1800 CE (Figure 6). Therefore, we believe that Labrador Sea influences decreased throughout LIA due to NAO^-, leading to the further increase in temperature and oxygen isotope signal.

The end of the time interval (~1810-1870 CE), coincides with the early stage of the industrial era (~1830 CE onwards), both reconstructed air temperature and sea surface temperature recorded a <0.2 °C and <0.5 °C increase respectively (Abram et al., 2016). However, the climate-related warming could not explain the ~2 °C increase observed in bottom water temperature compared to the start of this interval. Therefore, the warming could be mainly caused by the further increased presence of ATSW and the weaker contribution of LSSW. The timing of the peak matched the end of the large-scale ice-rafting events in ~1800 CE (Alonso-Garcia et al., 2017), and the end of the series of volcanic eruptions (~1835 CE) (Brönnimann et al., 2019). Therefore, less freshwater should be entering the Labrador Current thus weakening the LSSW. Moreover, the Gulf Stream transport has been observed to increase since 1850, contributing to the increase in ATSW contribution. A decrease in the DWBC was also observed from sortable silt (Thornalley et al., 2018), leading to further decrease in LSSW contribution, explaining the maximum oxygen isotopic signal observed in this time interval.

Post-LIA (~1871 CE onward)

449 The start of this interval was marked by a sharp decrease of more than 3°C in bottom water
450 temperature, suggesting a major change in the parent water mass contribution, and that was
451 followed by fluctuations in both temperature and oxygen isotope signal until the end of the
452 analysis. This seemed to be contradictory to a previous finding that suggested an increasing
453 trend in the Gulf Stream transport at this time interval (Lund et al., 2006). The observed drop
454 in oxygen isotope signal may be explained by an increase in the proportion of LSSW entering
455 the Laurentian channel or by a decrease in the isotopic signature of the parent water masses.
456 Given that the surface temperature started to go up after the LIA (Abram et al., 2016), it was
457 possible to deduce a stronger freshwater discharge from the post-LIA sea ice melting, thus a
458 stronger Labrador Current and LSSW contribution (Thibodeau et al. 2018), as evidenced by a
459 sudden increase in arctic ice export observed in another study (Alonso-Garcia et al., 2017). A
460 previous study also observed a drop of ~0.3‰ in seawater oxygen isotope signal in the Gulf
461 Stream at this time (Lund et al., 2006), which would explain 50% of the signal by itself. In
462 short, the observed sudden drop in oxygen isotope signal could be explained by an increased
463 Labrador Current discharge and/or lower oxygen isotope signals from the Gulf Stream and
464 potentially the Labrador Current due to freshwater input following the LIA and/or more
465 positive NAO (Trouet, Scourse, and Raible 2012).
466
467 To deduce whether the isotopic signal of the parent water masses has been altered towards
468 more depleted values, a cross-plot of reconstructed temperature and $\delta^{18}O_{(seawater)}$ was shown
469 in Figure 7. With the theoretical seawater oxygen isotope signal of ATSW and LSSW to be
470 0.5‰ and -0.5 ‰ respectively (Thibodeau et al. 2018), the curve for the post-LIA interval
471 shown in Figure 7 was observed to be more negative than the other time intervals, serving as
472 a piece of evidence to our post-1850 CE freshwater input hypothesis.
473

Parent Water Mass Contribution as potential proxy of AMOC strength

Interestingly, the records produced here mostly reproduced the general trend observed in the AMOC index from Rahmstorf et al. 2015 (Figure 6), i.e., a general decline in AMOC which coincide with an increase in the proportion of ATSW entering the Laurentian Channel, which is coherent with previous hypothesis (Thibodeau et al. 2018). While the similarity in patterns highlight the potential of using parent water mass contribution as a proxy for the strength of AMOC, our findings highlight the importance of using a multiproxy approach, in this case coupling $\delta^{18}O$ with Mg/Ca to better disentangle the different potential signals and their drivers. While our record generally follows the predicted trend during the LIA the relationship does not stand after 1850 when AMOC weakens while we observed a shift toward a higher proportion of LSSW.

CONCLUSION

In this paper, we have used single foraminifer ICP-MS to establish an exponential Mg/Ca-temperature calibration curve for *Globobulimina auriculata* at the Lower St. Lawrence Estuary, i.e. $Mg/Ca\ (mmol/mol) = 0.6341e^{(0.3740t)}$. This bottom water temperature reconstruction curve can be used for a temperature range from 3.0 to 5.5°C. Despite its narrow temperature range, it provides a more species- and region-specific curve for more accurate temperature reconstruction in future studies.

Using the newly established calibration curve and Mg/Ca obtained from the MD99-2220 core, we reconstructed the bottom water temperature at the Lower St. Lawrence Estuary during LIA. Constrained with $\delta^{18}O_{(calcite)}$ data, we calculated the $\delta^{18}O_{(seawater)}$ change and used it as a proxy for the parent water mass contribution change. From our result, we linked the oceanographic changes in LIA with volcanism, solar irradiance and negative North Atlantic

Oscillation condition. We observed a similarity between our records and previous proxy interpretations on the strength of AMOC, Gulf Stream and Labrador Current, indicating the potential of using parent water mass contribution to St. Lawrence Estuary to infer regional oceanographical change. In our proxy result, we interpreted a stepwise weakening of AMOC throughout LIA followed by a drastic disruption of oxygen isotope signal potentially from freshwater forcing. Considering the potential AMOC weakening to be induced from global warming, our study may provide insights into the driving forces of the atmospheric-oceanic response involved.

ACKNOWLEDGEMENT

This study was funded through the General Research Fund from the Research Grant Council of Hong Kong (#17301320) awarded to Benoit Thibodeau. The authors thank the technical support provided by Mr Cho On Thomas Tang from the Chinese University of Hong Kong for ICPMS measurements.

DATA AVAILABILITY

Data will be available at https://doi.org/10.48668/HLKYYR upon acceptance of the paper.

REFERENCES

Abram, N.J., McGregor, H.V., Tierney, J.E., Evans, M.N., McKay, N.P., Kaufman, D.S., 2016. Early onset of industrial-era warming across the oceans and continents. Nature 536, 411–418. https://doi.org/10.1038/nature19082

Agilent Technologies, 2014. Agilent 7900 ICP-MS MassHunter Workstation User Guide.

Alkhatib, M., Qutob, M., Alkhatib, S., Eisenhauer, A., 2022. Influence of precipitation rate and temperature on the partitioning of magnesium and strontium in calcite overgrowths. Chemical Geology 599, 120841. https://doi.org/10.1016/j.chemgeo.2022.120841

Alonso-Garcia, M., Kleiven, H. (Kikki) F., McManus, J.F., Moffa-Sanchez, P., Broecker, W.S., Flower, B.P., 2017. Freshening of the Labrador Sea as a trigger for Little Ice Age development. Climate of the Past 13, 317–331. https://doi.org/10.5194/cp-13-317-2017

Anand, P., Elderfield, H., Conte, M.H., 2003. Calibration of Mg/Ca thermometry in planktonic foraminifera from a sediment trap time series. Paleoceanography 18. https://doi.org/10.1029/2002PA000846

Barker, S., Greaves, M., Elderfield, H., 2003. A study of cleaning procedures used for foraminiferal Mg/Ca paleothermometry. Geochemistry, Geophysics, Geosystems 4. https://doi.org/10.1029/2003GC000559

Barrientos, N., Lear, C.H., Jakobsson, M., Stranne, C., O'Regan, M., Cronin, T.M., Gukov, A.Y., Coxall, H.K., 2018. Arctic Ocean benthic foraminifera Mg/Ca ratios and global Mg/Ca-temperature calibrations: New constraints at low temperatures. Geochimica et Cosmochimica Acta, Chemistry of oceans past and present: A Special Issue in tribute to Harry Elderfield 236, 240–259. https://doi.org/10.1016/j.gca.2018.02.036

Behringer, W., 1999. Climatic Change and Witch-hunting: the Impact of the Little Ice Age on Mentalities. Climatic Change 43, 335–351. https://doi.org/10.1023/A:1005554519604

Bentov, S., Erez, J., 2006. Impact of biomineralization processes on the Mg content of foraminiferal shells: A biological perspective. Geochemistry, Geophysics, Geosystems 7. https://doi.org/10.1029/2005GC001015

Bonnet, R., Swingedouw, D., Gastineau, G., Boucher, O., Deshayes, J., Hourdin, F., Mignot, J., Servonnat, J., Sima, A., 2021. Increased risk of near term global warming due to a recent AMOC weakening. Nat Commun 12, 6108. https://doi.org/10.1038/s41467-021-26370-0

Broecker, W.S., Peng, T.-H., 1982. Tracers in the Sea. Lamont-Doherty Geological Observatory, Columbia University Palisades, New York.

Brönnimann, S., Franke, J., Nussbaumer, S.U., Zumbühl, H.J., Steiner, D., Trachsel, M., Hegerl, G.C., Schurer, A., Worni, M., Malik, A., Flückiger, J., Raible, C.C., 2019. Last phase of the Little Ice Age forced by volcanic eruptions. Nat. Geosci. 12, 650–656. https://doi.org/10.1038/s41561-019-0402-y

Buckley, M.W., Marshall, J., 2016. Observations, inferences, and mechanisms of the Atlantic Meridional Overturning Circulation: A review. Reviews of Geophysics 54, 5–63. https://doi.org/10.1002/2015RG000493

Dawson, A.G., Hickey, K., Mayewski, P.A., Nesje, A., 2007. Greenland (GISP2) ice core and historical indicators of complex North Atlantic climate changes during the fourteenth century: Holocene. Holocene 17, 427–434. https://doi.org/10.1177/0959683607077010

Ditlevsen, P., Ditlevsen, S., 2023. Warning of a forthcoming collapse of the Atlantic meridional overturning circulation. Nat Commun 14, 4254. https://doi.org/10.1038/s41467-023-39810-w

Elderfield, H., Yu, J., Anand, P., Kiefer, T., Nyland, B., 2006. Calibrations for benthic foraminiferal Mg/Ca paleothermometry and the carbonate ion hypothesis. Earth and Planetary Science Letters 250, 633–649. https://doi.org/10.1016/j.epsl.2006.07.041

Erez, J., 2003. The Source of Ions for Biomineralization in Foraminifera and Their Implications for Paleoceanographic Proxies. Reviews in Mineralogy and Geochemistry 54, 115–149. https://doi.org/10.2113/0540115

Evans, D., Sagoo, N., Renema, W., Cotton, L.J., Müller, W., Todd, J.A., Saraswati, P.K., Stassen, P., Ziegler, M., Pearson, P.N., Valdes, P.J., Affek, H.P., 2018. Eocene greenhouse climate revealed by coupled clumped isotope-Mg/Ca thermometry. Proceedings of the National Academy of Sciences of the United States of America 115, 1174–1179.

Ezer, T., 2015. Detecting changes in the transport of the Gulf Stream and the Atlantic overturning circulation from coastal sea level data: The extreme decline in 2009–2010 and estimated variations for 1935–2012. Global and Planetary Change 129, 23–36. https://doi.org/10.1016/j.gloplacha.2015.03.002

Fan, K., 2023. The Little Ice Age and the Fall of the Ming Dynasty: A Review. Climate 11, 71. https://doi.org/10.3390/cli11030071

Ferreira, D., Marshall, J., Campin, J.-M., 2010. Localization of Deep Water Formation: Role of Atmospheric Moisture Transport and Geometrical Constraints on Ocean Circulation. Journal of Climate 23, 1456–1476. https://doi.org/10.1175/2009JCLI3197.1

Galaasen, E.V., Ninnemann, U.S., Kessler, A., Irvalı, N., Rosenthal, Y., Tjiputra, J., Bouttes, N., Roche, D.M., Kleiven, H. (Kikki) F., Hodell, D.A., 2020. Interglacial instability of North Atlantic Deep Water ventilation. Science 367, 1485–1489. https://doi.org/10.1126/science.aay6381

Galbraith, P.S., Chassé, J., Caverhill, C., Nicot, P., Gilbert, D., Lefaivre, D., Lafleur, C., n.d. Physical Oceanographic Conditions in the Gulf of St. Lawrence during 2017.

Holliday, N.P., Bersch, M., Berx, B., Chafik, L., Cunningham, S., Florindo-López, C., Hátún, H., Johns, W., Josey, S.A., Larsen, K.M.H., Mulet, S., Oltmanns, M., Reverdin, G., Rossby, T., Thierry, V., Valdimarsson, H., Yashayaev, I., 2020. Ocean circulation causes the largest freshening event for 120 years in eastern subpolar North Atlantic. Nat Commun 11, 585. https://doi.org/10.1038/s41467-020-14474-y

Hoogakker, B., Elderfield, H., Oliver, K., Crowhurst, S., 2010. Benthic foraminiferal oxygen isotope offsets over the last glacial-interglacial cycle. Paleoceanography 25. https://doi.org/10.1029/2009PA001870

Jackson, L.C., Kahana, R., Graham, T., Ringer, M.A., Woollings, T., Mecking, J.V., Wood, R.A., 2015. Global and European climate impacts of a slowdown of the AMOC in a high resolution GCM. Clim Dyn 45, 3299–3316. https://doi.org/10.1007/s00382-015-2540-2

Jackson, S., Sylvester, P., 2008. Calibration strategies for elemental analysis. Signal 10, 100.

John, E.H., Staudigel, P.T., Buse, B., Lear, C.H., Pearson, P.N., Slater, S.M., 2023. Revealing Their True Stripes: Mg/Ca Banding in the Paleogene Planktonic Foraminifera Genus Morozovella and Implications for Paleothermometry. Paleoceanography and Paleoclimatology 38, e2023PA004652. https://doi.org/10.1029/2023PA004652

Jutras, M., Dufour, C.O., Mucci, A., Talbot, L.C., 2023. Large-scale control of the retroflection of the Labrador Current. Nat Commun 14, 2623. https://doi.org/10.1038/s41467-023-38321-y

Katz, A., 1973. The interaction of magnesium with calcite during crystal growth at 25–90°C and one atmosphere. Geochimica et Cosmochimica Acta 37, 1563–1586. https://doi.org/10.1016/0016-7037(73)90091-4

Knudsen, M.F., Jacobsen, B.H., Seidenkrantz, M.-S., Olsen, J., 2014. Evidence for external forcing of the Atlantic Multidecadal Oscillation since termination of the Little Ice Age. Nat Commun 5, 3323. https://doi.org/10.1038/ncomms4323

Lapointe, F., Bradley, R.S., 2021. Little Ice Age abruptly triggered by intrusion of Atlantic waters into the Nordic Seas. Science Advances 7, eabi8230. https://doi.org/10.1126/sciadv.abi8230

Lean, J., Rind, D., 1999. Evaluating sun–climate relationships since the Little Ice Age. Journal of Atmospheric and Solar-Terrestrial Physics 61, 25–36. https://doi.org/10.1016/S1364-6826(98)00113-8

Lear, C.H., Rosenthal, Y., Slowey, N., 2002. Benthic foraminiferal Mg/Ca-paleothermometry: a revised core-top calibration. Geochimica et Cosmochimica Acta 66, 3375–3387. https://doi.org/10.1016/S0016-7037(02)00941-9

Lobelle, D., Beaulieu, C., Livina, V., Sévellec, F., Frajka-Williams, E., 2020. Detectability of an AMOC Decline in Current and Projected Climate Changes. Geophysical Research Letters 47, e2020GL089974. https://doi.org/10.1029/2020GL089974

Lund, D.C., Lynch-Stieglitz, J., Curry, W.B., 2006. Gulf Stream density structure and transport during the past millennium. Nature 444, 601–604. https://doi.org/10.1038/nature05277

Martin, P.A., Lea, D.W., 2002. A simple evaluation of cleaning procedures on fossil benthic foraminiferal Mg/Ca. Geochemistry, Geophysics, Geosystems 3, 1–8. https://doi.org/10.1029/2001GC000280

Mathien-Blard, E., Bassinot, F., 2009. Salinity bias on the foraminifera Mg/Ca thermometry: Correction procedure and implications for past ocean hydrographic reconstructions. Geochemistry, Geophysics, Geosystems: G3 10. https://doi.org/10.1029/2008GC002353

Mayewski, P.A., Meeker, L.D., Twickler, M.S., Whitlow, S., Yang, Q., Lyons, W.B., Prentice, M., 1997. Major features and forcing of high-latitude northern hemisphere atmospheric circulation using a 110,000-year-long glaciochemical series. Journal of Geophysical Research: Oceans 102, 26345–26366. https://doi.org/10.1029/96JC03365

Miller, G.H., Geirsdóttir, Á., Zhong, Y., Larsen, D.J., Otto-Bliesner, B.L., Holland, M.M., Bailey, D.A., Refsnider, K.A., Lehman, S.J., Southon, J.R., Anderson, C., Björnsson, H., Thordarson, T., 2012. Abrupt onset of the Little Ice Age triggered by volcanism and sustained by sea-ice/ocean feedbacks. Geophysical Research Letters 39. https://doi.org/10.1029/2011GL050168

Moffa-Sánchez, P., Hall, I.R., 2017. North Atlantic variability and its links to European climate over the last 3000 years. Nat Commun 8, 1726. https://doi.org/10.1038/s41467-017-01884-8

Moffa-Sánchez, P., Hall, I.R., Barker, S., Thornalley, D.J.R., Yashayaev, I., 2014. Surface changes in the eastern Labrador Sea around the onset of the Little Ice Age. Paleoceanography 29, 160–175. https://doi.org/10.1002/2013PA002523

Moffa-Sánchez, P., Moreno-Chamarro, E., Reynolds, D.J., Ortega, P., Cunningham, L., Swingedouw, D., Amrhein, D.E., Halfar, J., Jonkers, L., Jungclaus, J.H., Perner, K., Wanamaker, A., Yeager, S., 2019. Variability in the Northern North Atlantic and Arctic Oceans Across the Last Two Millennia: A Review. Paleoceanography and Paleoclimatology 34, 1399–1436. https://doi.org/10.1029/2018PA003508

Mucci, A., 1987. Influence of temperature on the composition of magnesian calcite overgrowths precipitated from seawater. Geochimica et Cosmochimica Acta 51, 1977–1984. https://doi.org/10.1016/0016-7037(87)90186-4

Perner, K., Moros, M., Lloyd, J.M., Kuijpers, A., Telford, R.J., Harff, J., 2011. Centennial scale benthic foraminiferal record of late Holocene oceanographic variability in Disko Bugt, West Greenland. Quaternary Science Reviews 30, 2815–2826. https://doi.org/10.1016/j.quascirev.2011.06.018

Putnam, A.E., Putnam, D.E., Andreu-Hayles, L., Cook, E.R., Palmer, J.G., Clark, E.H., Wang, C., Chen, F., Denton, G.H., Boyle, D.P., Bassett, S.D., Birkel, S.D., Martin-Fernandez, J., Hajdas, I., Southon, J., Garner, C.B., Cheng, H., Broecker, W.S., 2016. Little Ice Age wetting of interior Asian deserts and the rise of the Mongol Empire. Quaternary Science Reviews 131, 33–50. https://doi.org/10.1016/j.quascirev.2015.10.033

Rahmstorf, S., Box, J.E., Feulner, G., Mann, M.E., Robinson, A., Rutherford, S., Schaffernicht, E.J., 2015. Exceptional twentieth-century slowdown in Atlantic Ocean overturning circulation. Nature Clim Change 5, 475–480. https://doi.org/10.1038/nclimate2554

Rashid, H., Piper, D.J.W., Lazar, K.B., McDonald, K., Saint-Ange, F., 2017. The Holocene Labrador Current: Changing linkages to atmospheric and oceanographic forcing factors. Paleoceanography 32, 498–510. https://doi.org/10.1002/2016PA003051

Rashid, H., Zhang, Z., Piper, D.J.W., Patro, R., Xu, Y., 2023. Impact of Medieval Climate Anomaly and Little Ice Age on the Labrador Current flow speed and the AMOC reconstructed by the sediment dynamics and biomarker proxies. Palaeogeography, Palaeoclimatology, Palaeoecology 111558. https://doi.org/10.1016/j.palaeo.2023.111558

Rosenthal, Y., Boyle, E.A., Slowey, N., 1997. Temperature control on the incorporation of magnesium, strontium, fluorine, and cadmium into benthic foraminiferal shells from Little Bahama Bank: Prospects for thermocline paleoceanography. Geochimica et Cosmochimica Acta 61, 3633–3643. https://doi.org/10.1016/S0016-7037(97)00181-6

Rustic, G.T., Polissar, P.J., Ravelo, A.C., DeMenocal, P., 2021. Relationship between individual chamber and whole shell Mg/Ca ratios in Trilobatus sacculifer and implications for individual foraminifera palaeoceanographic reconstructions. Scientific Reports (Nature Publisher Group) 11. https://doi.org/10.1038/s41598-020-80673-8

Saenger, C., Chang, P., Ji, L., Oppo, D.W., Cohen, A.L., 2009. Tropical Atlantic climate response to low-latitude and extratropical sea-surface temperature: A Little Ice Age perspective. Geophysical Research Letters 36. https://doi.org/10.1029/2009GL038677

Segnit, E.R., Holland, H.D., Biscardi, C.J., 1962. The solubility of calcite in aqueous solutions—I The solubility of calcite in water between 75° and 200° at CO2 pressures up to 60 atm. Geochimica et Cosmochimica Acta 26, 1301–1331. https://doi.org/10.1016/0016-7037(62)90057-1

Sicre, M.-A., Weckström, K., Seidenkrantz, M.-S., Kuijpers, A., Benetti, M., Masse, G., Ezat, U., Schmidt, S., Bouloubassi, I., Olsen, J., Khodri, M., Mignot, J., 2014. Labrador current variability over the last 2000 years. Earth and Planetary Science Letters 400, 26–32. https://doi.org/10.1016/j.epsl.2014.05.016

Stirpe, C.R., Allen, K.A., Sikes, E.L., Zhou, X., Rosenthal, Y., Cruz-Uribe, A.M., Brooks, H.L., 2021. The Mg/Ca proxy for temperature: A Uvigerina core-top study in the Southwest Pacific. Geochimica et Cosmochimica Acta 309, 299–312. https://doi.org/10.1016/j.gca.2021.06.015

St-Onge, G., Stoner, J.S., Hillaire-Marcel, C., 2003. Holocene paleomagnetic records from the St. Lawrence Estuary, eastern Canada: centennial- to millennial-scale geomagnetic modulation of cosmogenic isotopes. Earth and Planetary Science Letters 209, 113–130. https://doi.org/10.1016/S0012-821X(03)00079-7

Thibodeau, B., de Vernal, A., Hillaire-Marcel, C., Mucci, A., 2010. Twentieth century warming in deep waters of the Gulf of St. Lawrence: A unique feature of the last millennium. Geophysical Research Letters 37. https://doi.org/10.1029/2010GL044771

Thibodeau, B., de Vernal, A., Mucci, A., 2006. Recent eutrophication and consequent hypoxia in the bottom waters of the Lower St. Lawrence Estuary: Micropaleontological and geochemical evidence. Marine Geology 231, 37–50. https://doi.org/10.1016/j.margeo.2006.05.010

Thibodeau, B., Not, C., Zhu, J., Schmittner, A., Noone, D., Tabor, C., Zhang, J., Liu, Z., 2018. Last Century Warming Over the Canadian Atlantic Shelves Linked to Weak Atlantic Meridional Overturning Circulation. Geophys. Res. Lett. 45, 12,376-12,385. https://doi.org/10.1029/2018GL080083

Thornalley, D.J.R., Oppo, D.W., Ortega, P., Robson, J.I., Brierley, C.M., Davis, R., Hall, I.R., Moffa-Sanchez, P., Rose, N.L., Spooner, P.T., Yashayaev, I., Keigwin, L.D., 2018. Anomalously weak Labrador Sea convection and Atlantic overturning during the past 150 years. Nature 556, 227–230. https://doi.org/10.1038/s41586-018-0007-4

Trejos, T., Montero, S., Almirall, J.R., 2003. Analysis and comparison of glass fragments by laser ablation inductively coupled plasma mass spectrometry (LA-ICP-MS) and ICP-MS. Anal Bioanal Chem 376, 1255–1264. https://doi.org/10.1007/s00216-003-1968-0

Trouet, V., Scourse, J.D., Raible, C.C., 2012. North Atlantic storminess and Atlantic Meridional Overturning Circulation during the last Millennium: Reconciling contradictory proxy records of NAO variability. Global and Planetary Change, Perspectives on Climate in Medieval Time 84–85, 48–55. https://doi.org/10.1016/j.gloplacha.2011.10.003

Wanner, H., Pfister, C., Neukom, R., 2022. The variable European Little Ice Age. Quaternary Science Reviews 287, 107531. https://doi.org/10.1016/j.quascirev.2022.107531

Weldeab, S., Arce, A., Kasten, S., 2016. Mg/Ca-ΔCO3porewater2−–temperature calibration for Globobulimina spp.: A sensitive paleothermometer for deep-sea temperature reconstruction. Earth and Planetary Science Letters 438, 95–102. https://doi.org/10.1016/j.epsl.2016.01.009

Yoshimura, T., Tanimizu, M., Inoue, M., Suzuki, A., Iwasaki, N., Kawahata, H., 2011. Mg isotope fractionation in biogenic carbonates of deep-sea coral, benthic foraminifera, and hermatypic coral. Anal Bioanal Chem 401, 2755–2769. https://doi.org/10.1007/s00216-011-5264-0

Zhou, X., Hess, A.V., Bu, K., Sagawa, T., Rosenthal, Y., 2022. Simultaneous Determination of I/Ca and Other Elemental Ratios in Foraminifera: Comparing Results From Acidic and Basic Solutions. Geochemistry, Geophysics, Geosystems 23, e2022GC010660. https://doi.org/10.1029/2022GC010660

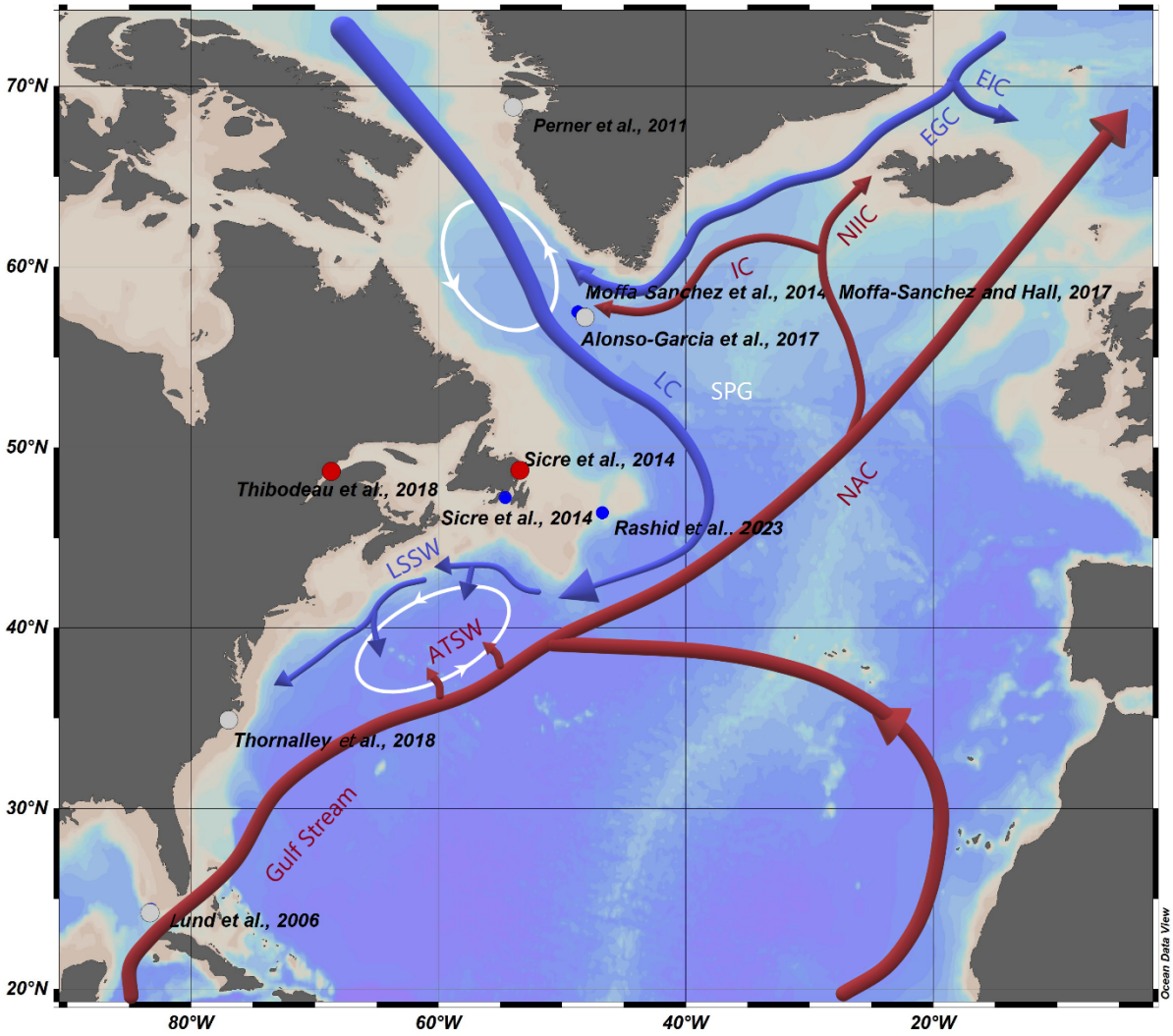

Figure 1 Map of North Atlantic, ocean currents and locations of study cores listed in Table 1. Red dots refer to studies indicating a warming during LIA, blue dots refer to studies indicating a cooling during LIA while grey dots refer to studies studying non-temperature-related proxies. Abbreviations on the map are: ATSW= Atlantic Temperate Slope Water; EIC= East Iceland Current; EGC= East Greenland Current; IC= Irminger Current; LC= Labrador Current; LSSW: Labrador Sea Slope Water; NAC= North Atlantic Current; NIIC= North Iceland Irminger Current; SPG= sub-polar gyre; The two white circles indicate convection; the upper one refers to Labrador Sea Convection while the lower one refers to Northern Recirculation Gyre.

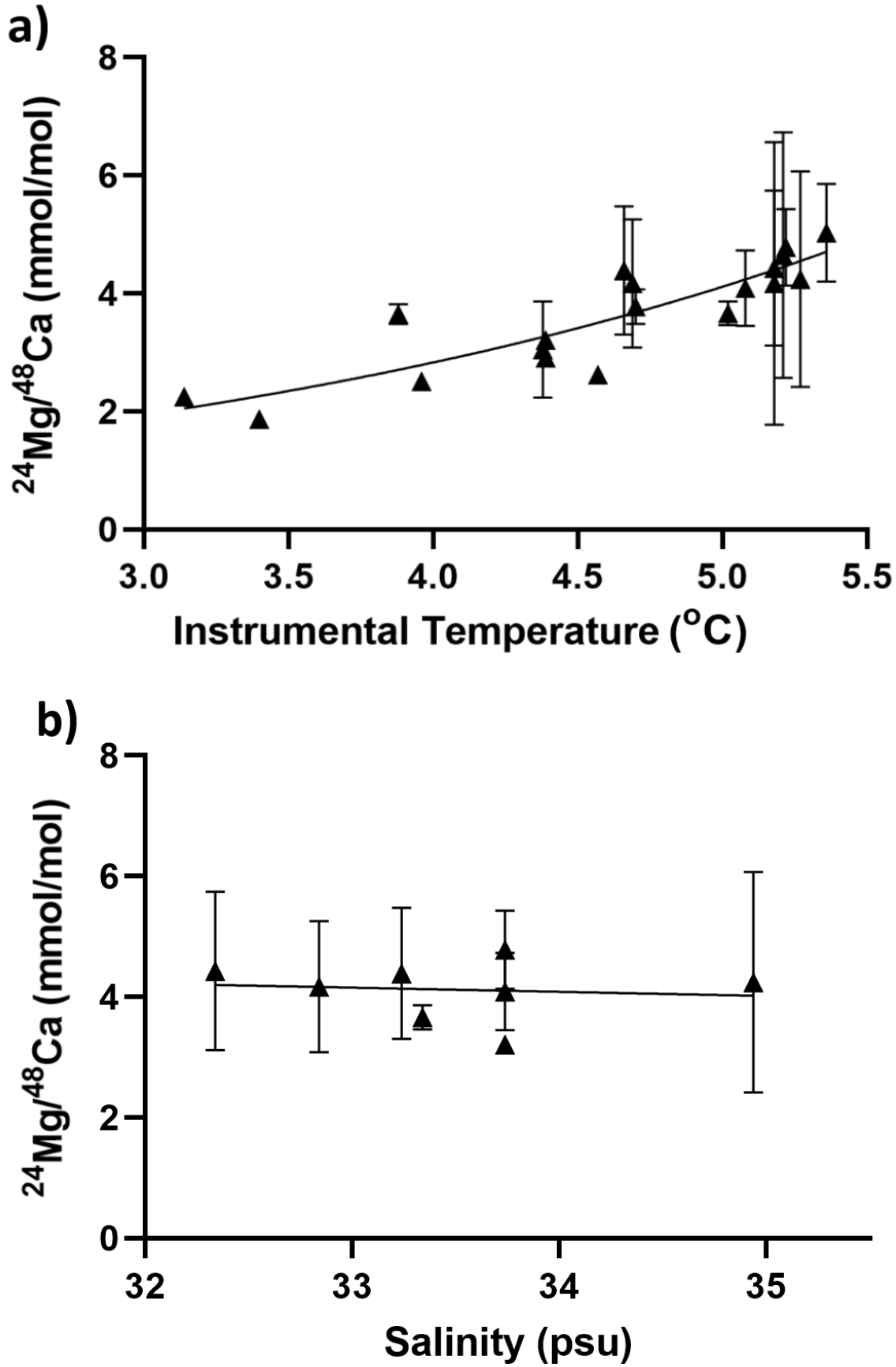
a)
$^{24}Mg/^{48}Ca$ (mmol/mol)
0
2
4
6
8
3.0
3.5
4.0
4.5
5.0
5.5
Instrumental Temperature (°C)
b)
$^{24}Mg/^{48}Ca$ (mmol/mol)
0
2
4
6
8
32
33
34
35
Salinity (psu)

765 Figure 2 Best-fit curve for the MeRC-corrected 24Mg/48Ca data against a)instrumental temperature
766 and b) instrumental salinity respectively. Error bars were indicated as standard deviations.

767

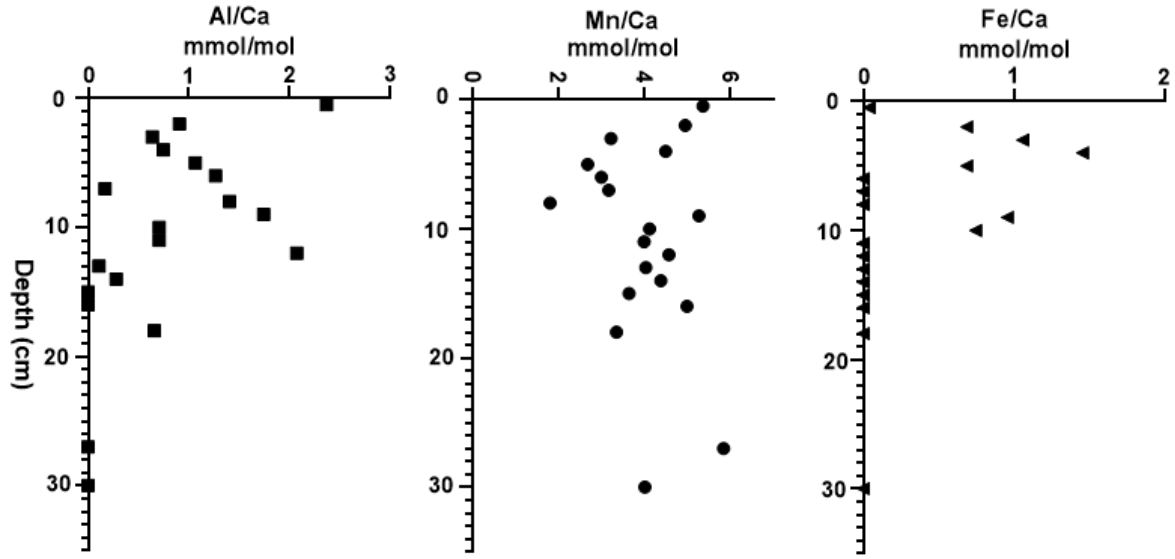

768

769 Figure 3 Contaminant/Ca ratio downcore

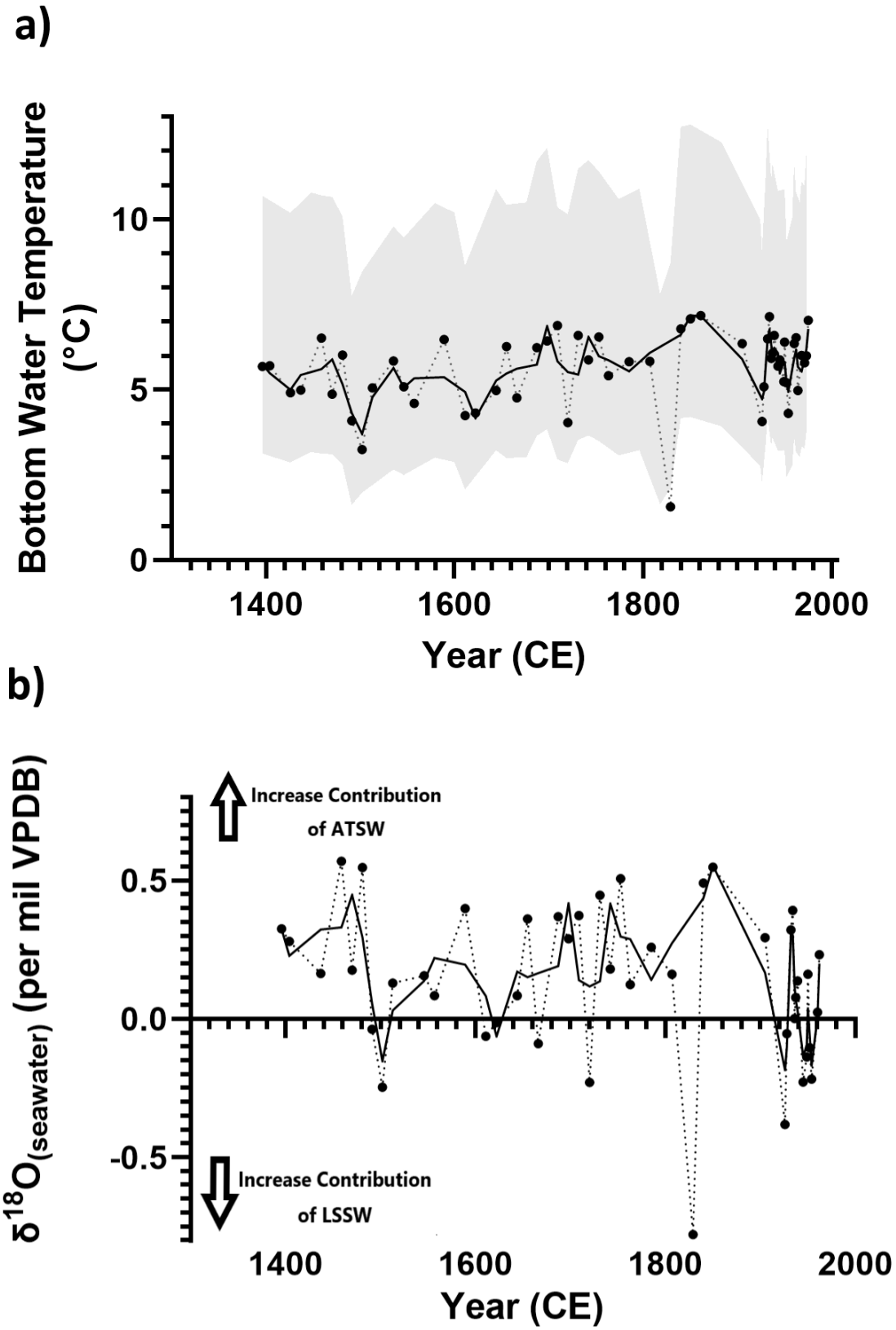

Figure 4 a) Bottom Water Temperature Reconstruction and b) seawater oxygen isotope reconstruction of the St. Lawrence Estuary from 1396 to 1975 CE. The trend lines were drawn with second order smoothing 5-point moving average. The light dotted line

represented the connecting curve of all data points. Temperature uncertainty was set as a 95% of the confidence interval equation fit of the 2-period moving average, excluding the data point at 1829 CE.

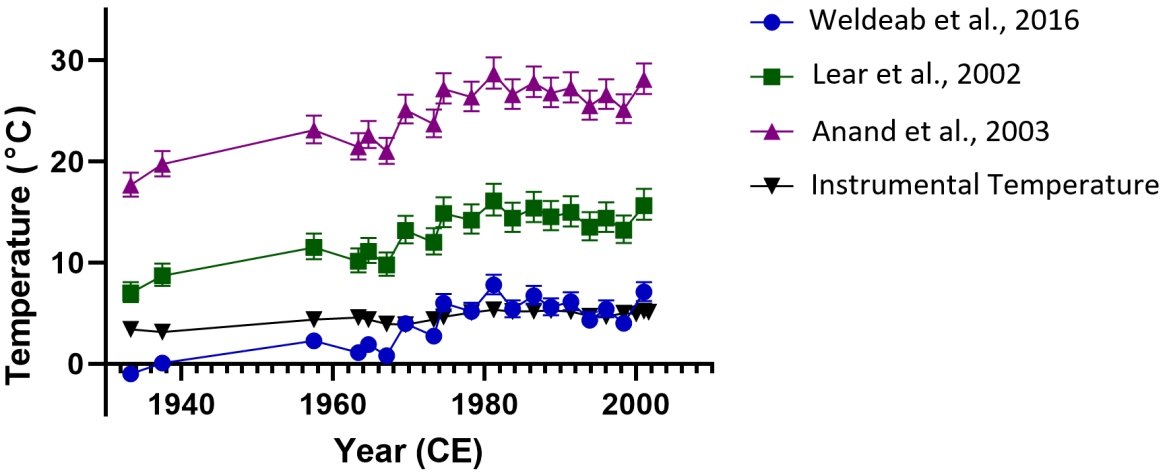

Figure 5 Bottom water temperature reconstruction from MeRC corrected $^{24}Mg/^{48}Ca$ data. Black curve with dot: Reconstruction from Weldeab, Arce, and Kasten 2016; Green curve with square: Lear, Rosenthal, and Slowey 2002; Purple curve with triangle: Anand, Elderfield, and Conte 2003. Error bars are represented as the maximum and minimum value from their equations.

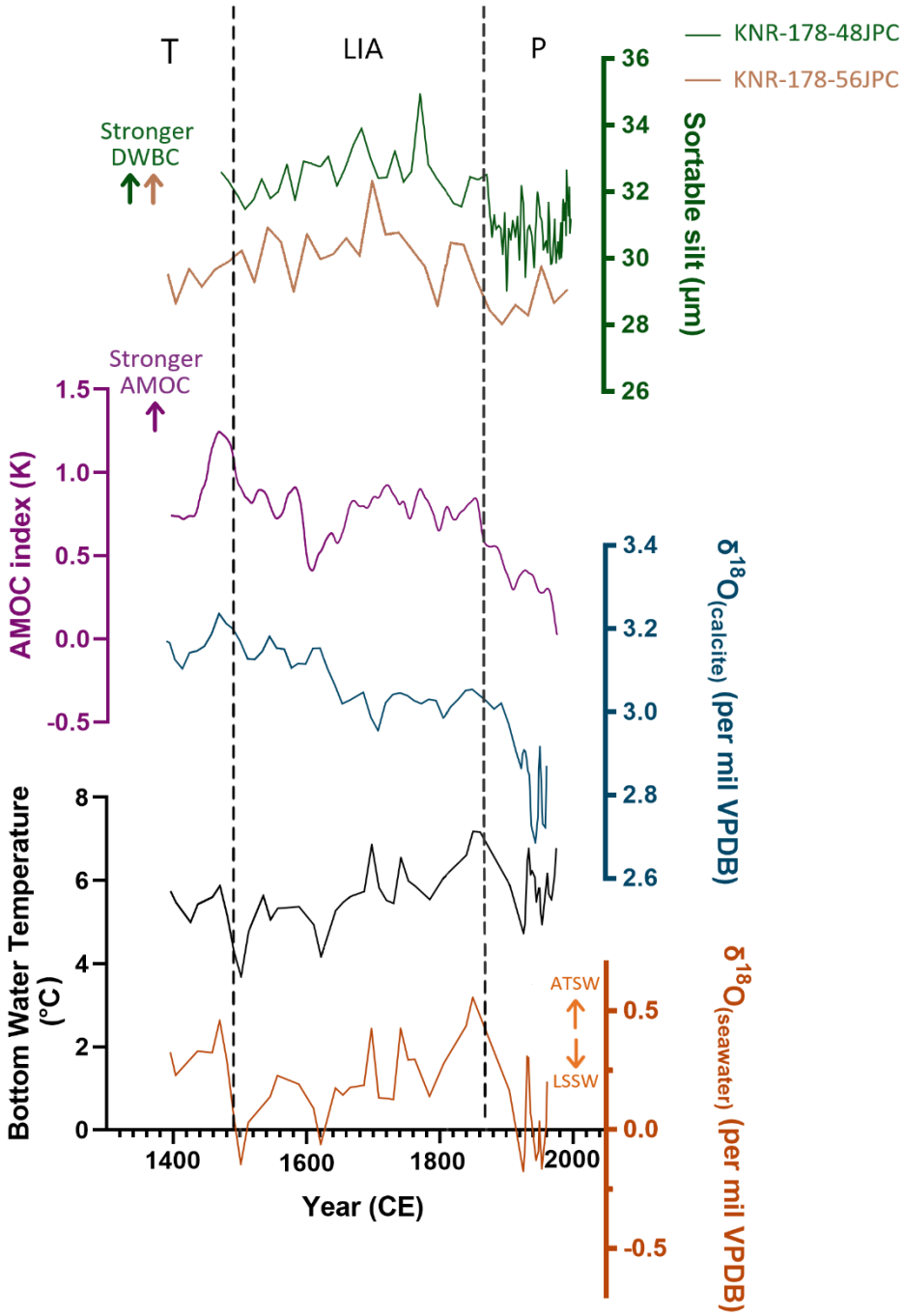

Figure 6 Comparison of previous LIA records with our proxy result. Green (KNR-178-48JPC) and brown (KNR-178-56JPC): Sortable silt as a proxy of flow speed of deep western boundary current (Thornalley et al. 2018); Purple: smoothened AMOC index (second degree smoothening, 25 neighbours on each side) (Rahmstorf et al. 2015); Dark blue: $\delta^{18}O$ *G. auriculata* (MD99-2220) (Thibodeau et al. 2018); Black: Bottom water reconstruction from MD99-2220 (this study); Orange: Seawater $\delta^{18}O$ reconstruction (this study). The black vertical dashed lines indicate the suggested separation between different time intervals. T = Transition; LIA= Little Ice Age; P= Post-LIA.

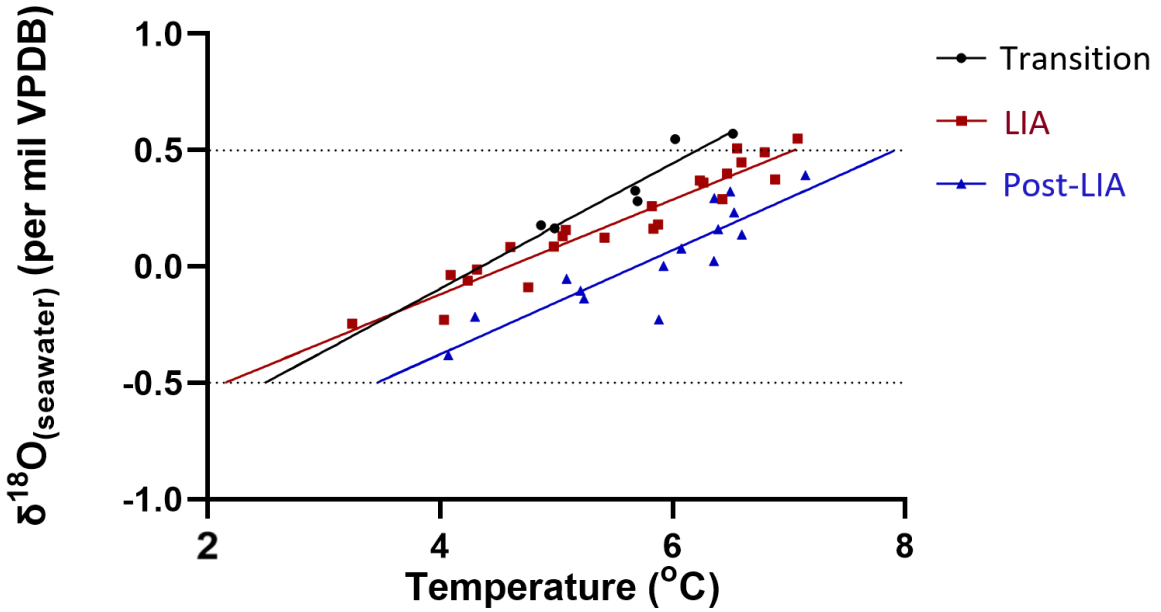

Figure 7 Cross plot of reconstructed temperature v.s. reconstructed oxygen isotope. Black dots represent points obtained in the Transitional interval (1396-1490 CE); Red rectangles represent points obtained during LIA (1491-1870 CE); Blue triangles represent points obtained in the post-LIA interval (1871 – 1975 CE). The corresponding colour lines represent the respective linear regression obtained.

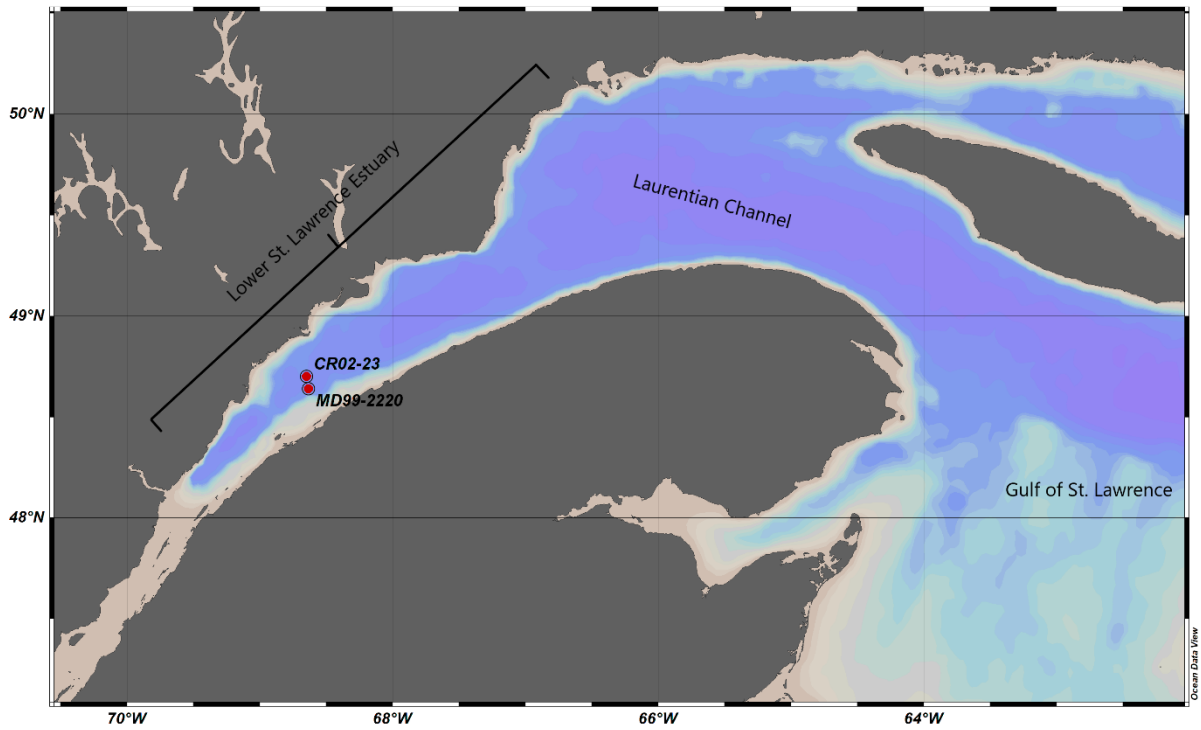

Supplementary Figure 1 Map of the St. Lawrence Estuary. Red dots indicate the location of the study cores (MD99-2220 and CR02-23).

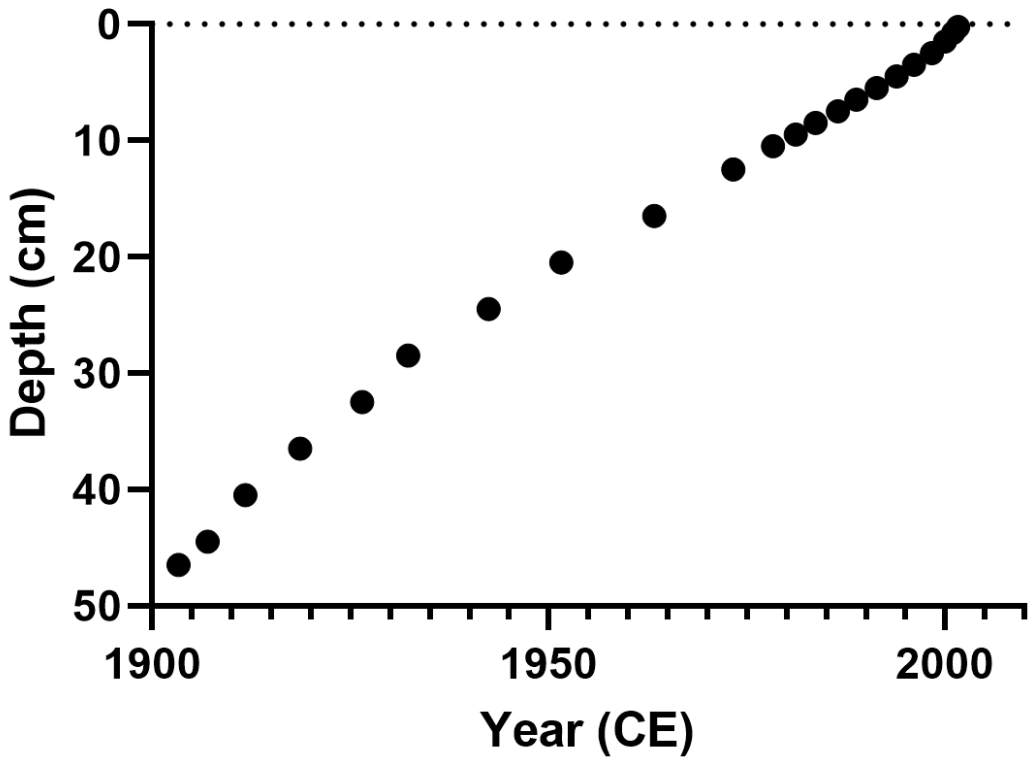

Supplementary Figure 2 Age Model of CR02-23, adopted from Thibodeau et al. 2018

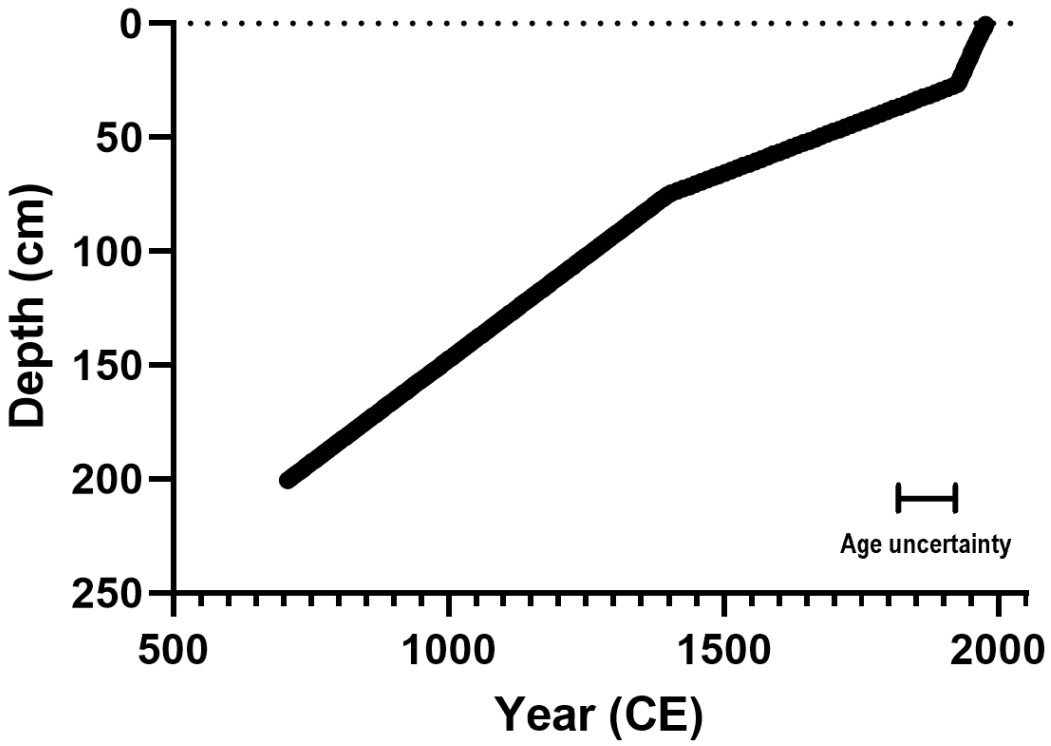

806
807 Supplementary Figure 3 Age model of MD99-2220. Adopted from Thibodeau et al., 2018.

808
809

810

811 Table 1. Summary of previous marine sediment proxy studies regarding oceanographic
812 changes in NW Atlantic during the LIA.

Ocean Layer	Study	Core	Proxy	Result	Oceanographic Interpretation	Timing
Sea ice	Alonso-Garcia et al. 2017	GS06-144-03	Ice-drafted debris	More ice-rafting events before the onset and during LIA	Cooling in LIA caused by previous Arctic freshwater discharges to the Labrador Sea in MCA	Pre and during LIA; ~1000–1100, ~1150–1250, ~1400–1450, ~1650–1700, ~1750–1800 CE
Near surface	Moffa-Sánchez et al. 2014	RAPiD-35-COM	δ18O; Mg/Ca; foraminifera assemblage	Lower SST of the eastern Labrador Sea; higher abundance of N. pachyderma	Increased influence of Polar Water; decreased influence of Atlantic Water in the Labrador Sea	During LIA; ~1400–1900 CE
Surface	Sicre et al. 2014	AI07-04BC, AI07-03G, AI07-11BC, AI07-12G	δ18O; Alkenone	Warmer SST along NE Newfoundland	Reduction of Labrador Sea convection; Labrador Current weakening; less freshwater contribution to Labrador Current	~1350 CE–present
Surface	Perner et al. 2011	MSM343310	Benthic foraminifera assemblage	Increasing influence of polar waters into West Greenland Current	(Atmospheric interpretation) NAO- condition during LIA	Starting in 1050 CE; highest influence at ~1650 CE
Near surface	Rashid et al. 2023	MO2009061-0217	TEX86	Abrupt cooling at ~1350 CE; warming at ~1400 CE; cooling at ~1450 CE	Warming induced by reduction in subpolar gyre and Labrador Sea; cooling induced by	~1350–1750 CE

Ocean Layer	Study	Core	Proxy	Result	Oceanographic Interpretation	Timing
					increasing polar water influence	
Near-bottom	Rashid et al. 2023	MO2009061-0217	Sortable silt	Flow rate of Labrador Current was faster in LIA	Labrador Current more vigorous in LIA; increasing rate from ~1400–1600 CE and ~1640–1700 CE	~1400–1700 CE (peaks as noted)
Near bottom	Moffa-Sánchez & Hall 2017	RAPiD-35-COM; RAPiD-21-COM	Foraminifera assemblage; sortable silt	More polar water entering Labrador Sea; reduced Labrador Sea Water in Iceland Basin	Reducing subpolar gyre strength	During LIA; ~1400–1900 CE
Near bottom	Thornalley et al. 2018	48JPC, 56JPC	Sortable silt	A decrease in flow speed of the deep western boundary current	Weakened Labrador Sea convection and AMOC at the end of LIA	At the end of LIA; after 1850 CE
Bottom water	Thibodeau et al. 2018	MD99-2220	Benthic δ18O	Lower oxygen isotope signal	More contribution to St. Lawrence Estuary from Labrador Current during LIA	Mid to end of LIA; ~1600–1900 CE
Whole water column	Lund, Lynch-Stieglitz, & Curry 2006	50MC-E; 49GGC; 16MC-A; 3MC-H; W167-79GGC; 62MC-A; 11MC-D	Planktic and benthic δ18O	Lower density gradient and vertical current shear of the Gulf Stream	Weaker Gulf Stream during LIA	Pre and during LIA; ~1200–1850 CE

Table S2. Elimination threshold for data elimination in ICP-MS.

Ratio or concentration	Threshold (mmol/mol or ppb)
Al/Ca	5.5
Mn/Ca	6
Ca	500 ppb
Mg/Ca	10
Fe/Ca	5

Table S3. Average and standard deviation of Mg/Ca ratio in each depth of core CR23-23 after MeRC correction with the corresponding instrumental temperature described in Thibodeau et al., 2018. NA (not applicable) refers to average with only one measurement left in the depth and unavailable data for salinity. Values (except depth) were corrected to two decimal places.

Depth (cm)	$^{24}Mg/^{48}Ca$ (mmol/mol)		Instrumental Temperature (°C) (Thibodeau et al., 2018)	Instrumental salinity (psu) (Galbraith et al., 2018)
	Average	Standard Deviation		
0.5-1	4.78	0.65	5.22	33.74
2-3	3.66	0.20	5.02	33.34
3-4	4.17	1.09	4.69	32.84
4-5	3.78	0.30	4.7	NA
5-6	4.43	1.31	5.18	32.34
6-7	4.24	1.83	5.27	34.94
7-8	4.65	2.08	5.21	NA
8-9	4.17	2.39	5.18	NA
9-10	5.03	0.83	5.36	NA
10-11	4.09	0.64	5.08	33.74
11-12	4.39	1.09	4.66	33.24
12-13	3.21	0.15	4.39	33.74
13-14	3.65	0.17	3.88	NA
14-15	2.51	NA	3.96	NA
15-16	2.91	0.04	4.39	NA
16-17	2.62	NA	4.57	NA
18-19	3.05	0.81	4.38	NA
27-28	2.25	NA	3.14	NA

30-31	1.87	0.15	3.4	NA

Table S4. Comparison of best-fit curve on $^{24}Mg/^{48}Ca$ after MeRC correction. Standard errors are used as errors of the linear equations *(Bryan & Marchitto, 2008)*; 95% confidence interval was used as errors for the exponential equations *(Lea et al., 1999)*. p-values were calculated as the 95% confidence interval. t= bottom water temperature in °C. Values in equations are corrected to 4 significant figures.

	$^{24}Mg/^{48}Ca$ (mmol/mol)
Best-fit Equation (Exponential)	$Mg/Ca = 0.6341e^{(0.3740t)}$
Range of equation in 95% CI profile	Maximum: $Mg/Ca = 1.114e^{(0.5008t)}$ Minimum: $Mg/Ca = 0.3399\ e^{(0.2574t)}$
R-square	0.76
Degrees of Freedom	19
Percentage of Mg/Ca increase per 1°C increase	45.35%
Linear Equation	$Mg/Ca = (1.217 \pm 0.1746)t - (1.959 \pm 0.8132)$
R-square	0.74
p-value	<0.0001 (significant)
Mg/Ca increase per 1°C increase	1.22 mmol/mol

Table S5. Linear and Exponential fit correlating 300 m deep water salinity data (Galbraith et al., 2018) and two treatments of $^{24}Mg/^{48}Ca$ data. The "s" in equation represents 300m bottom water salinity. P-value was calculated with a 95% confidence interval. Standard error was used as the uncertainty of the linear equation. "NA" = not applicable. t represents water temperature in Celsius.

Linear Fit	$^{24}Mg/^{48}Ca$ (mmol/mol) vs salinity	Difference between $^{24}Mg/^{48}Ca$ (mmol/mol) and back-calculated Mg/Ca (mmol/mol) from Weldeab, Arce, and Kasten 2016 against salinity (psu)
Equation	$Mg/Ca = (-0.06881 \pm 0.2578)s - (6.426 \pm 8.635)$	$Mg/Ca = (-0.1049 \pm 0.2229)s + (3.634 \pm 7.467)$
R-square	0.01	0.04
p-value	0.80 (not significant)	0.65 (not significant)
Exponential Fit		
Equation	$Mg/Ca = 7.411e^{(-0.01752t)}$	Data too unstable for calculation
Range of equation in 95% CI profile	Maximum: $Mg/Ca = 1653e^{(0.1366t))}$ Minimum: $Mg/Ca = 0.04178\ e^{(-0.1796t)}$	NA
R-square	0.01	NA
Degree of Freedom	6	6

Table S6 Mann-Kendall trend test and Sens's slope test on year 1490-1870 CE. A 95% confidence interval was se

Mann-Kendall Trend Test (Reconstructed $\delta^{18}O_{(seawater)}$)	
Time frame	1490-1870 CE
z-score	2.01
Sens' slope	0.016 (positive trend)
Number of samples	24
p-value	0.04 (significant)
Mann-Kendall Trend Test (Reconstructed Temperature)	
Time frame	1490-1870 CE
z-score	2.97
Sens' slope	0.097 (positive trend)
Number of samples	25
p-value	<0.01 (significant)